ROYAL SOCIETY
OF CHEMISTRY

PAPER

Check for updates

A polarized luminescence thermometer based on a dye encapsulated metal–organic framework†

Shenghan Lin,‡[a] Zhengluan Liao,‡[a] Heqi Zheng,[a] Chenyu Li,[a] Yuanjing Cui, [ID] ★[ab]
Zhiyu Wang [ID] [a] and Guodong Qian [ID] ★[a]

Temperature is a central concept within the realm of thermodynamics and statistics. Extensive research has been dedicated to luminescence metal–organic framework (MOF) thermometers with adjustable emission. Nevertheless, the majority of the reported ratiometric MOF thermometers rely on multiple luminescent centers that produce dual emission. This reliance on lanthanides raises concerns related to cost implications and potential supply shortages. Polarized luminescence thermometers offer distinct advantages as they are less susceptible to variations in probe concentrations and irradiation conditions. Herein, we successfully establish efficient host–guest systems for polarized luminescence thermometers by encapsulating dyes within the metal–organic framework (MOF) ZJU-28. Due to the alignment of chromophores within MOFs, these systems exhibit polarized luminescence and temperature sensing properties. The synthesized composites, specifically ZJU-28⊃DSM, enable self-referenced temperature sensing in the range from 293 K to 305 K with a sensitivity of 0.025% K^{-1}, while ZJU-28⊃ACF covers a wide temperature sensing range albeit with a decreased sensitivity. Considering the wealth of porous MOFs and emitting units available, the proposed approach can be extended to other luminescent MOFs by adjusting their pore size and employing different organic dyes, opening up a new perspective for the design of host–guest MOF⊃dye polarized luminescence thermometers.

Introduction

Temperature is considered the most fundamental thermodynamic state variable and remains one of the most regularly measured key quantities across various fields of science and technology. In the context of the contact-based readout principle, it becomes imperative to establish direct thermal contact between the actual detector and the sample; however, this has the potential to disrupt processes within micro- and nanoscale systems.[1,2] In contrast to traditional contact thermometers, luminescence thermometers present a promising thermal sensing method due to their resistance to electromagnetic interference, high-voltage insulation capabilities, stability, reliability, long lifespan, corrosion resistance, and high sensitivity.[3–6] Moreover, it offers the advantage of being noninvasive, providing real-time thermal

readings, and boasting high spatial temperature resolution.[6,7] Luminescence thermometers rely on temperature-dependent optical signals to determine the local temperature around a phosphor. This measurement, known as a thermometric parameter ($\Delta(T)$), encompasses various aspects such as the intensity of a single band, luminescence intensity ratio, polarization-based emission ratio, decay time, rise time, and band energy or width.[8] Thus far, the operation of many luminescence thermometers has been primarily based on a single optical signal. This approach often necessitates recalibration in complex environments due to variations in the physicochemical characteristics among luminophores. A more dependable thermometer can be achieved by incorporating multiple optical signals, such as lanthanide ions based on energy transfer within the framework of solids or temperature-sensitive fluorescent dyes, into the materials. This approach enables mutual verification between the optical signals.[9–16]
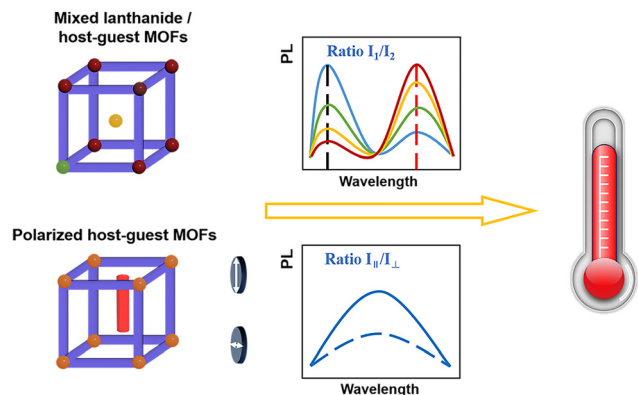
Metal–organic frameworks (MOFs) are excellent candidates as luminescent materials due to the vast array of their available metal ions and organic linkers, offering nearly unlimited choices.[17–23] The luminescence of MOFs can be engineered by the regulation of ligand design, metal ion selection and encapsulation of guest molecules within the MOF cavity. Lanthanide-based MOFs exhibit multi-emissive and self-referencing sensor behaviors.[24,25] Apart from the lanthanide metal ions,

[a] *State Key Laboratory of Silicon and Advanced Semiconductor Materials,*
School of Materials Science & Engineering, Zhejiang University, Hangzhou 310027,
China. E-mail: gdqian@zju.edu.cn

[b] *ZJU-Hangzhou Global Scientific and Technological Innovation Center,*
Zhejiang University, Hangzhou 311215, China. E-mail: cuiyj@zju.edu.cn

† Electronic supplementary information (ESI) available: Materials and methods, emission spectra, canonical score plots and linear regression curves of sensor arrays, additional SEM, NMR, TGA, FT-IR figures, *etc.* See DOI: https://doi.org/10.1039/d3tc04532c

‡ These authors contributed equally to this paper.

This journal is © The Royal Society of Chemistry 2024

J. Mater. Chem. C, 2024, **12**, 2391–2397 | **2391**

Scheme 1 Schematic diagram of the traditional ratiometric luminescence thermometer based on the luminescence intensity ratio and the polarized luminescence thermometer based on the luminescence polarization ratio.

Fig. 1 Encapsulation of DSM and ACF dyes into ZJU-28 *via* an ion-exchange process.

the inclusion of a dye or quantum dots within the channels of MOFs makes it possible to fabricate a MOF thermometer. Furthermore, the channel structure of MOFs provides an ideal spatial confinement for the assembly and separation of organic guest molecules. This strategy effectively reduces intermolecular interactions and improves luminescence stability, all while preserving sensitive temperature dependence.[26–29] However, most prominently cited MOF thermometers in the literature rely heavily on incorporating photoactive lanthanides. This raises concerns regarding both cost implications and the possibility of supply shortages. Furthermore, conventional ratiometric MOF ⊃ dye thermometers usually necessitate the incorporation of two distinct luminescent centers within the MOF, which poses a challenge in the fabrication of composite materials (Scheme 1).

Polarized luminescence thermometers rely on the temperature-dependent polarization state of luminescence emitted by luminescent molecules undergoing Brownian dynamics.[30–33] When a luminescent molecule is illuminated using a linearly polarized laser beam, it emits partially polarized luminescence due to the random molecular orientation. The explanation for this phenomenon arises from the variability in the orientation of the absorption transition dipole moment orientation in response to temperature fluctuations.[34] Polarized luminescence thermometers offer the advantages of remote monitoring, self-referencing, fast response time and non-contact measurement.[35] However, in conventional polarization luminescence thermometry, the attachment of fluorophores to proteins is required to constrain their rotation, enhancing fluorescence anisotropy for temperature detection. This practice limits the range of applications for polarization luminescence thermometry.

In prior studies, porous metal–organic frameworks have been employed to confine dye molecules or create aligned luminescent ligands, thereby achieving polarized emission.[36–40] Taking the composite ZJU-68 ⊃ DSM (4-[*p*-(dimethylamino)styryl]-1-methylpyridinium, DSM) as an example, owing to the highly oriented assembly of dye molecules within the channels of ZJU-68, it exhibits perfect emission polarization with its degree of polarization exceeding 99.9%.[37]
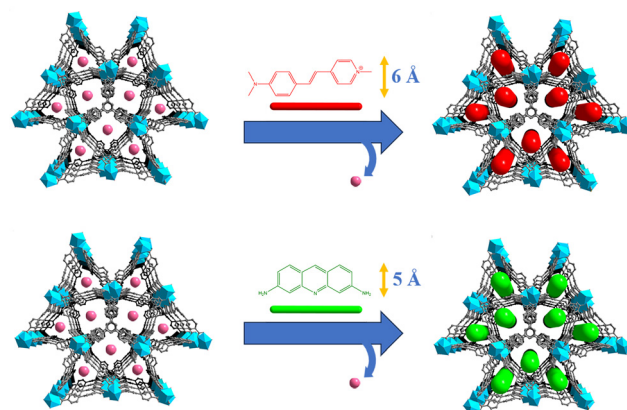
Consequently, the incorporation of dyes into suitably sized one-dimensional (1D) channels of a MOF to form a host–guest MOF has become a well-established method for attaining polarized emission. This method leverages the alignment of these linear molecules, resulting in the strongest signal along their orientation and the weakest signal perpendicular to their orientation.[41] While MOFs with polarizing properties have found applications in anti-counterfeiting, second-harmonic generation, and various other fields, a polarized luminescence thermometer based on MOFs has yet to be developed.[42,43]

Herein, MOF ⊃ dye polarized luminescence thermometers were realized by introducing a linear dye into the 1D channels of the MOF. In this case, ZJU-28 (ZJU-28 = [In$_3$(BTB)$_4$](Me$_2$NH$_2$)$_3$) was chosen as the host MOF based on our previous work.[44] This MOF features appropriately sized 1D channels for guest encapsulation. To restrain the rotation of dyes, they were encapsulated within the channels of ZJU-28. Recognizing that the choice of different sizes may impact temperature sensing properties, linear dye molecules, namely 4-[*p*-(dimethylamino)styryl]-1-methylpyridinium (DSM) and acriflavine (ACF), were introduced as guests into the 1D channels of ZJU-28 (Fig. 1). In this way, an increase in temperature led to a decrease in the emission polarization ratio of the dyes encapsulated in channels of ZJU-28. Accordingly, ZJU-28 ⊃ dye composites exhibited a change in polarization ratio in response to temperature, making it an ideal candidate for polarized luminescence thermometers.

Results and discussion

The reaction of InCl$_3$·4H$_2$O with the tritopic carboxylate ligand H$_3$BTB in *N,N*-dimethylformamide (DMF), 1,4-dioxane, H$_2$O and nitric acid formed a porous MOF ZJU-28. Within ZJU-28, two distinct types of 1D channels were described along the *c*-axis, measuring approximately 6.1 × 6.1 Å^2 and 7.1 × 8.5 Å^2, respectively (Fig. S1, ESI†). These channels and void spaces were occupied by a significant amount of highly disordered solvent and cationic Me$_2$NH$_2^+$ molecules with an evaluated crystal volume of 64.7%.[44] The space filling model structures

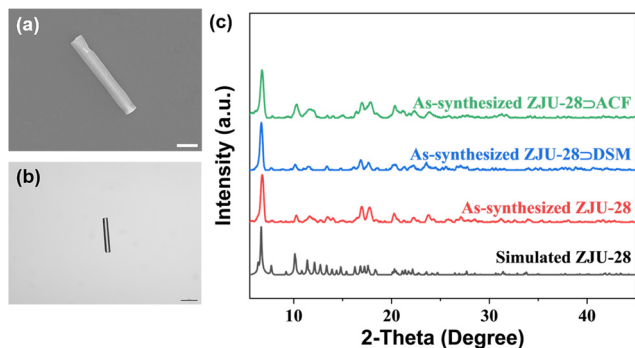**2392** | *J. Mater. Chem. C*, 2024, **12**, 2391–2397

This journal is © The Royal Society of Chemistry 2024

Fig. 2 (a) SEM image of ZJU-28. Scale bar: 20 μm. (b) Optical micrographs of ZJU-28. Scale bar: 20 μm. (c) PXRD patterns of simulated ZJU-28, as-synthesized ZJU-28, and as-synthesized composites ZJU-28⊃DSM and ZJU-28⊃ACF.

of DSM and ACF molecules demonstrate widths of approximately 6 Å and 5 Å, respectively, making them suitable for incorporating into the 1D channels of ZJU-28 (Fig. S2, ESI†). To introduce dyes into the channels of ZJU-28, MOF crystals were immersed in dimethylformamide (DMF) solutions containing cationic dyes DSM and ACF at temperature for approximately 8 hours. The resulting samples were filtered, thoroughly washed with DMF and EtOH until no characteristic emission was observed in the filtrate upon excitation, and then air-dried. The exchange reaction involving $Me_2NH_2^+$ cations and DSM and ACF dyes led to a noticeable change in the color of the ZJU-28 crystals, producing the composites ZJU-28⊃DSM and ZJU-28⊃ACF. The size and morphology of the prepared materials were examined using scanning electron microscopy (Fig. 2a) and optical microscopy (Fig. 2b). ZJU-28 crystals exhibited a distinctive triangular prism morphology with a smooth and pristine surface (Fig. 2b). The phase purity of obtained crystals was confirmed *via* powder X-ray diffraction (PXRD) analysis. The measured data concurred with the simulated results (Fig. 2c). The PXRD data corresponding to these dye-exchanged MOFs closely resembled those of the original ZJU-28 MOF, indicating that the ion exchange process preserved the integrity of the crystal structure. The ion exchange experiment was carried out under ambient environmental conditions without any atmospheric protection, making the formation and composition regulation of ZJU-28⊃dye composites straightforward.

Using UV-Vis spectroscopy, the concentrations of DSM and ACF were determined to be about 29.08 wt% and 21.05 wt% (Fig. S3, ESI†). To further confirm that the dyes were encapsulated into the channels of MOF crystals, a confocal laser scanning microscopy (CLSM) experiment was conducted using a single crystal in a depth scanning mode. In this mode, a single crystal was imaged by systematically adjusting the depth to produce a series of optical slice images. The luminescence emitted by the dyes was observed throughout the whole volume of the MOF crystal, thus confirming that the dye was encapsulated into the channels of ZJU-28 rather than being adsorbed on the surface (Fig. S4, ESI†). This observation provided evidence that the *c*-axis (corresponding to the longitudinal direction) of

the ZJU-28 crystal aligned with the 1D channels. Furthermore, Fourier transform infra-red (FTIR) spectra and ¹H nuclear magnetic resonance results also corroborated the presence of DSM molecules within the structure of ZJU-28⊃DSM. Upon ion-exchange treatment, ZJU-28⊃DSM and ZJU-28⊃ACF emerged a noticeable absorption peak at 1163 cm⁻¹ and 1608 cm⁻¹ in comparison to ZJU-28, respectively, corresponding to the vibrational absorption of DSM and ACF (Fig. S5 and S6, ESI†).

The thermogravimetric analysis (TGA) curves of ZJU-28, ZJU-28⊃DSM and ZJU-28⊃ACF were found to each display two distinct weight loss events (Fig. S7, ESI†). The first weight loss, occurring from room temperature to 400 °C, corresponds to the loss of solvent and water and the second weight loss at about 400 °C can be attributed to the decomposition of organic ligands and dyes. These results demonstrate the good thermal stability of ZJU-28, ZJU-28⊃DSM and ZJU-28⊃ACF. Furthermore, this host–guest MOF exhibits good chemical stability (Fig. S8, ESI†).

Subsequently, the fluorescence properties and the photoluminescence quantum fields (PLQYs) of ZJU-28, ZJU-28⊃DSM, ZJU-28⊃ACF and DSM and ACF dyes in DMF solution at room temperature were investigated. ZJU-28 exhibited distinct absorption bands with a peak at 340 nm (Fig. S9, ESI†), while ZJU-28⊃DSM and ZJU-28⊃ACF revealed new absorption bands peaking at 532 nm and 467 nm, respectively, attributed to the absorption of DSM and ACF dyes (Fig. S10, ESI†). A comparison of the fluorescence properties was conducted among ZJU-28, DSM solution in DMF and ZJU-28⊃DSM (Fig. S11, ESI†). When excited at 532 nm, ZJU-28 exhibited negligible emission with a PLQY of approximately 0% (Table S1, ESI†). In contrast, ZJU-28⊃DSM demonstrated a robust emission ($\Phi \approx 27.41\%$). Meanwhile, the DSM solution showed a faint red emission ($\Phi \approx 0.14\%$). When excited at 467 nm, ZJU-28 also displayed minimal emission, characterized by a PLQY of 0% (Table S2, ESI†). ZJU-28⊃ACF displayed strong emission with a significantly higher PLQY of 27.35% (Fig. S12, ESI†), while the ACF solution presented a relatively strong luminescence ($\Phi \approx 20.11\%$). These results demonstrate that MOF channels effectively suppressed aggregation of dyes, resulting in enhanced luminescence. It is widely recognized that the quantum yield of dyes in highly diluted solutions is remarkably improved; however, utilizing such diluted solutions as luminescence thermometers is unfeasible due to their volatility, low boiling point and poor manageability. By contrast, ZJU-28⊃dyes are in a powder form and possess the ability to overcome these drawbacks when used as luminescent temperature sensors.

The narrow 1D channels of ZJU-28 confine linear dye molecules, likely inducing the periodic alignment and resulting in high optical anisotropy. Given that only the 1D channels can encapsulate linear dyes, the ZJU-28⊃dye composites are anticipated to exhibit anisotropic emission. We employed a custom-built polarization fluorescence imaging system to observe the luminescence output of ZJU-28⊃dye crystals under different emission-detected polarization directions (Fig. S14, ESI†).

This journal is © The Royal Society of Chemistry 2024

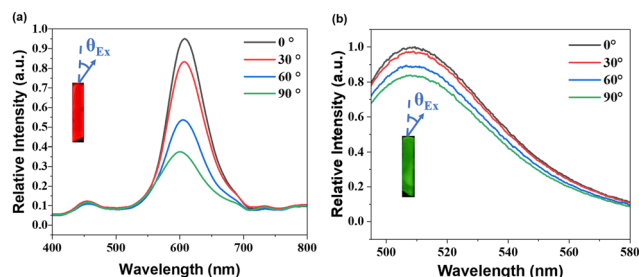*J. Mater. Chem. C*, 2024, **12**, 2391–2397 | **2393**

Fig. 3 The emission spectra of (a) a single ZJU-28⊃DSM crystal under an excitation of 532 nm and (b) a single ZJU-28⊃ACF crystal under an excitation of 467 nm when θ_{Ex} is changed. Inset: The measurement schematic diagram, where the blue arrows represent the excitation polarization.

When the emission-detected polarization direction was parallel to the longitudinal direction of the crystal, it resulted in the reception of the maximum number of photons, forming a bright imaging picture (Fig. S13(a), ESI†). In contrast, when the polarization direction was vertical, the numbers significantly decreased, leading to darker corresponding images (Fig. S13(b), ESI†). This anisotropic fluorescence phenomenon demonstrates that the dyes predominantly align along the longitudinal direction of the crystal, given that the absorption transition moment is approximately in the line with dye molecules.

The polarization of the output luminescence was investigated using the experimental setup depicted in Fig. S15 (ESI†). A highly polarized femtosecond (fs) laser with an operating wavelength of 532 nm was employed to excite the crystal. The resulting emission signals were meticulously captured using a high-resolution fiber optics spectrometer. Concurrently, the
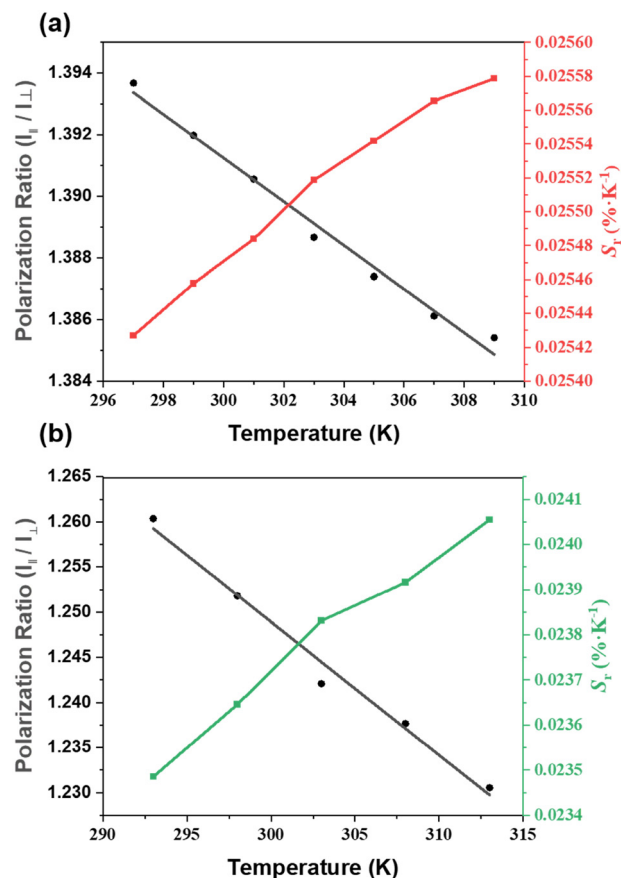

Fig. 5 The fitted curve of the temperature-dependent polarization ratio and the temperature-dependent relative sensitivity (S_r) of (a) ZJU-28⊃DSM between 297 K and 309 K and (b) ZJU-28⊃ACF between 293 K and 313 K.
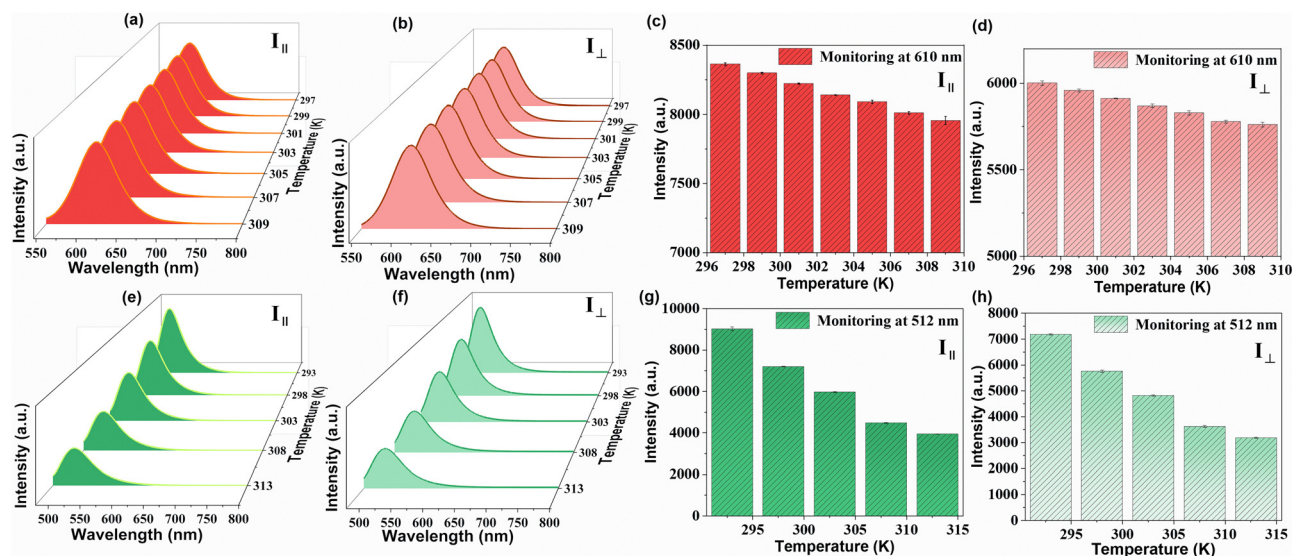

Fig. 4 Emission spectra of ZJU-28⊃DSM between 297 K and 309 K excited at 532 nm when the polarization direction is (a) parallel or (b) perpendicular to the excitation direction. The luminescence intensity monitoring at 610 nm of ZJU-28⊃DSM when the polarization is (c) parallel or (d) perpendicular to the excitation direction. Emission spectra of ZJU-28⊃ACF between 293 K and 313 K excited at 467 nm when the polarization direction is (e) parallel or (f) perpendicular to the excitation direction. The luminescence intensities monitoring at 512 nm of ZJU-28⊃ACF when the polarization is (g) parallel or (h) perpendicular to the excitation direction.

2394 | *J. Mater. Chem. C*, 2024, **12**, 2391–2397

This journal is © The Royal Society of Chemistry 2024

excited crystal gave a strong signal at 532 nm, accompanied by a broad and vibrant red emission. The emission light from the crystals was focused and collected with a fiber optic spectrometer. As shown in Fig. 3a and b, the intensity of one-photon emission diminished gradually as θ_{Ex} ranged from $0°$ to $90°$. This observation demonstrates the alignment of the absorption transition dipole moments of chromophores with the long axis of the crystal. The degree of polarization (DOP) was determined using the formula DOP = $(I_{max} - I_{min})/(I_{max} + I_{min})$, where I_{max} represents the intensity of the strongest polarization luminescence signals, and I_{min} corresponds to the intensity of the weakest signals.[45] The DOP values of ZJU-28⊃DSM and ZJU-28⊃ACF were approximately 37.13% and 10.1%, respectively.

Therefore, ZJU-28⊃DSM and ZJU-28⊃ACF composites in the powdered form also exhibit polarized luminescence properties.

As ZJU-28⊃DSM and ZJU-28⊃ACF presented polarized emission, we initiated the exploration of their potential as polarized luminescence thermometers. The experimental setup is depicted in Fig. S16 (ESI†). With the increase in the temperature of ZJU-28⊃DSM, the luminescence intensity decreased, regardless of whether the analyzer was aligned parallel or perpendicular to the polarizer (Fig. 4a–d). Meanwhile, ZJU-28⊃ACF displayed a similar trend (Fig. 4e and f). The variation in the ratio of the luminescence intensities of $I_\parallel$ and $I_\perp$ as a function of temperature is plotted in Fig. 5a and Fig. 5b, respectively. The correlation coefficient (R^2) was calculated to be 0.98, indicating a linear relationship between the polarization ratio of the luminescence intensity and temperature. The DOP values of ZJU-28⊃DSM at 297 K and 303 K are about 37.13% and 34.24%, respectively (Fig. S17, ESI†). To evaluate the reliability of temperature sensing, we exposed ZJU-28⊃ACF to three cycles from 293 K to 313 K (Fig. S18, ESI†). The alterations of the luminescence polarization ratio, which are temperature-dependent, exhibited complete reversibility. This suggests that the composite can be employed repeatedly.

The temperature sensing properties of ZJU-28⊃DSM and ZJU-28⊃ACF were investigated (Fig. 5a and b). Relativity sensitivity (S_r) is typically used for the quantitative evaluation of the performance of luminescence thermometers. It is defined as follows:

$$S_r = \left| \frac{\partial \Delta / \partial T}{\Delta} \right|$$

where Δ represents the measured temperature-sensitive parameter, and T is the temperature. Following this definition, the S_r of ZJU-28⊃DSM and ZJU-28⊃ACF exhibited a similar trend (Fig. 5a and b). With the increasing temperature, the S_r of two thermometers decreased. The maximum S_r values of ZJU-28⊃DSM and ZJU-28⊃ACF were determined to be 0.026% K^{-1} at 309 K and 0.024% K^{-1} at 313 K, respectively (Fig. 5a). In fact, when compared with ZJU-28⊃DSM, ZJU-28⊃ACF offers a broader temperature measurement range but exhibits relatively

insensitive temperature detection responses (Fig. 5b). This inspired us the range and sensitivity of temperature sensing in the ZJU-28⊃dye composite and polarized luminescence thermometers can be easily adjusted by encapsulating different dye molecules within the host framework, which is controlled through the dye-exchange process. With the inherent advantages of polarized light,[46] this approach holds the potential to emerge as a promising candidate as the temperature sensing material within biological organisms in the future.

Conclusions

In summary, we have successfully developed polarized luminescence thermometers by encapsulating dye molecules into the channels of the MOF. Given the importance of size and charge matching principles for the successful encapsulation of these dyes within the channels of the MOF material, we purposefully chose the readily available ZJU-28 as the host matrix and DSM and ACF dyes as the guest matrix. The confinement of dyes originating from ZJU-28 imparts polarization and temperature sensing properties to the ZJU-28⊃dye composites. As the temperature increases, the luminescence polarization ratio decreases. Compared to ZJU-28⊃DSM, the sensitivity and temperature sensing range changed while encapsulating ACF dyes within the channels of ZJU-28. These results underscore the advantages of the MOF encapsulation strategy, which includes the restriction of dye rotation and the enhancement of luminescence. Our work is expected to inspire further research in the design of novel polarization luminescence thermometers and provide deeper insights into such thermometers.

Experimental

Materials

All the reagents and chemicals were purchased from commercial sources and used directly without further purification. Indium chloride tetrahydrate (InCl$_3$·4H$_2$O, 99.99%), 1,3,5-tri(4-carboxyphenyl) benzene (H$_3$BTB, 98%), 4-[p-(dimethylamino)styryl]-1-methylpyridinium (DSM), acriflavine (ACF), N,N-dimethylformamide (DMF), 1,4-dioxane, deionized water, ethanol and other reagents were commercially available and used without further purification.

Synthesis of ZJU-28

ZJU-28 was synthesized based on our previous work with minor modification.[44] InCl$_3$·4H$_2$O (176 mg, 0.6 mmol) and H$_3$BTB (133 mg, 0.3 mmol) were dissolved in the solution of N,N-dimethylformamide (9 mL), 1,4-dioxane (6 mL), H$_2$O (1 mL) and nitric acid (63 μL). The resultant solution was sealed in a Teflon-lined stainless-steel bomb at 130 °C for 24 h. After cooling to room temperature, colorless ZJU-28 crystals of a needle-like morphology were collected by filtration, washed with DMF and dried in air.

This journal is © The Royal Society of Chemistry 2024

J. Mater. Chem. C, 2024, **12**, 2391–2397 | **2395**

Introduction of DSM into ZJU-28

The fresh ZJU-28 crystals (50 mg) were immersed in the DSM solution with a concentration of 5 mM at 60 °C. After several days, the red crystals of host–guest MOF ZJU-28 ⊃ DSM were obtained. They were then filtered off, washed several times with the fresh DMF and EtOH and dried in air.

Introduction of ACF into ZJU-28

The synthesis method was the same as that of ZJU-28 ⊃ DSM, just replaced the DSM solution with the same concentration of ACF solution to obtain yellow crystals ZJU-28 ⊃ ACF.

Polarization fluorescence imaging

All the polarization tests were performed on the *ac* plane (perpendicular to the *b*-axis) of the MOF crystal, which is owing to the thinness of the crystal and the limitation of instruments. A polarized picosecond laser of 405 nm was mounted on the laser launcher and coupled to the microscope (IX71, Olympus). The polarized direction of the 405 nm laser was kept parallel with the longitudinal direction of the ZJU-28 ⊃ DSM and ZJU-28 ⊃ ACF crystals. The emitting light from the crystals was passed through a main dichroic splitter and a linear polarizer. The signals were then collected using a single-photon counting detector (ID-100), and post analyzed by computer processing (Fig. S11, ESI†). By tuning the linear polarizer from parallel to vertical with the longitudinal direction of the crystal, the received signals vary from the maximum to minimum.

Other characterization methods

These results can be found in the Experimental section of the ESI.†

Author contributions

Conceptualization: Shenghan Lin, data curation: Shenghan Lin and Zhengluan Liao, formal analysis: Shenghan Lin and Heqi Zheng, funding acquisition: Yuanjing Cui and Guodong Qian, investigation: Shenghan Lin and Chenyu Li, methodology: Shenghan Lin and Zhiyu Wang, supervision: Yuanjing Cui and Guodong Qian, writing – original draft: Shenghan Lin, and writing – review and editing: Heqi Zheng, Yuanjing Cui, and Guodong Qian.

Conflicts of interest

There are no conflicts to declare.

Acknowledgements

References

1 M. R. Moldover, W. L. Tew and H. W. Yoon, *Nat. Phys.*, 2016, **12**, 7–11.

2 C. D. S. Brites, P. P. Lima, N. J. O. Silva, A. Millán, V. S. Amaral, F. Palacio and L. D. Carlos, *Adv. Mater.*, 2010, **22**, 4499–4504.

3 D. Jaque and F. Vetrone, *Nanoscale*, 2012, **4**, 4301.

4 C. D. S. Brites, S. Balabhadra and L. D. Carlos, *Adv. Opt. Mater.*, 2018, **7**, 1801239.

5 Z. Chen, K. Y. Zhang, X. Tong, Y. Liu, C. Hu, S. Liu, Q. Yu, Q. Zhao and W. Huang, *Adv. Funct. Mater.*, 2016, **26**, 4386–4396.

6 J. Zhou, B. del Rosal, D. Jaque, S. Uchiyama and D. Jin, *Nat. Methods*, 2020, **17**, 967–980.

7 S. Wang, M. Gong, X. Han, D. Zhao, J. Liu, Y. Lu, C. Li and B. Chen, *ACS Appl. Mater. Interfaces*, 2021, **13**, 11078–11088.

8 A. Bednarkiewicz, L. Marciniak, L. D. Carlos and D. Jaque, *Nanoscale*, 2020, **12**, 14405–14421.

9 T. Barilero, T. Le Saux, C. Gosse and L. Jullien, *Anal. Chem.*, 2009, **81**, 7988–8000.

10 Y. Cui, R. Song, J. Yu, M. Liu, Z. Wang, C. Wu, Y. Yang, Z. Wang, B. Chen and G. Qian, *Adv. Mater.*, 2015, **27**, 1420–1425.

11 J. Rocha, C. D. S. Brites and L. D. Carlos, *Chem. – Eur. J.*, 2016, **22**, 14782–14795.

12 L. Marciniak, K. Kniec, K. Elżbieciak-Piecka, K. Trejgis, J. Stefanska and M. Dramićanin, *Coord. Chem. Rev.*, 2022, **469**, 214671.

13 M. Xu, X. Zou, Q. Su, W. Yuan, C. Cao, Q. Wang, X. Zhu, W. Feng and F. Li, *Nat. Commun.*, 2018, **9**, 2698.

14 T. Feng, Y. Ye, X. Liu, H. Cui, Z. Li, Y. Zhang, B. Liang, H. Li and B. Chen, *Angew. Chem., Int. Ed.*, 2020, **59**, 21752–21757.

15 X. Rao, T. Song, J. Gao, Y. Cui, Y. Yang, C. Wu, B. Chen and G. Qian, *J. Am. Chem. Soc.*, 2013, **135**, 15559–15564.

16 Y. Gao, F. Huang, H. Lin, J. Zhou, J. Xu and Y. Wang, *Adv. Funct. Mater.*, 2016, **26**, 3139–3145.

17 H. Q. Zheng, Y. Yang, Z. Wang, D. Yang, G. Qian and Y. Cui, *Adv. Mater.*, 2023, **35**, 2300177.

18 Y. Cui, J. Zhang, H. He and G. Qian, *Chem. Soc. Rev.*, 2018, **47**, 5740–5785.

19 Y. Zhao, S. Qi, Z. Niu, Y. Peng, C. Shan, G. Verma, L. Wojtas, Z. Zhang, B. Zhang, Y. Feng, Y.-S. Chen and S. Ma, *J. Am. Chem. Soc.*, 2019, **141**, 14443–14450.

20 D.-G. Ha, R. Wan, C. A. Kim, T.-A. Lin, L. Yang, T. Van Voorhis, M. A. Baldo and M. Dincǎ, *Nat. Mater.*, 2022, **21**, 1275–1281.

21 X. Yang, X. Lin, Y. Zhao, Y. S. Zhao and D. Yan, *Angew. Chem., Int. Ed.*, 2017, **56**, 7853–7857.

22 S. Wang, Z. Ai, X. Niu, W. Yang, R. Kang, Z. Lin, A. Waseem, L. Jiao and H.-L. Jiang, *Adv. Mater.*, 2023, 2302512.

23 Y. Li, Q. Chen, L.-H. Xie, K. Wang, M. Zhao and J.-R. Li, *ACS Mater. Lett.*, 2022, **4**, 2345–2351.

24 Y. Cui, H. Xu, Y. Yue, Z. Guo, J. Yu, Z. Chen, J. Gao, Y. Yang, G. Qian and B. Chen, *J. Am. Chem. Soc.*, 2012, **134**, 3979–3982.

2396 | *J. Mater. Chem. C*, 2024, **12**, 2391–2397

This journal is © The Royal Society of Chemistry 2024

25 Z. Zhao, X. Shen, H. Li, K. Liu, H. Wu, X. Li and X. Gao, *Angew. Chem., Int. Ed.*, 2022, **61**, e202114340.

26 H. Cai, W. Lu, C. Yang, M. Zhang, M. Li, C.-M. Che and D. Li, *Adv. Opt. Mater.*, 2019, **7**, 1801149.

27 N. T. Trung, P. Q. Nhien, T. T. Kim Cuc, C.-H. Wu, B. T. Buu Hue, J. I. Wu, Y.-K. Li and H.-C. Lin, *ACS Appl. Mater. Interfaces*, 2023, **15**, 15353–15366.

28 H. Guan, M. Qi, L. Shi, W. Liu, L. Yang and W. Dou, *ACS Appl. Mater. Interfaces*, 2023, **15**, 18114–18124.

29 W. Cao, Y. Cui, Y. Yang and G. Qian, *ACS Mater. Lett.*, 2021, **3**, 1426–1432.

30 G. Baffou, M. P. Kreuzer, F. Kulzer and R. Quidant, *Opt. Express*, 2009, **17**, 3291–3298.

31 J. S. Donner, S. A. Thompson, M. P. Kreuzer, G. Baffou and R. Quidant, *Nano Lett.*, 2012, **12**, 2107–2111.

32 J. S. Donner, S. A. Thompson, C. Alonso-Ortega, J. Morales, L. G. Rico, S. I. C. O. Santos and R. Quidant, *ACS Nano*, 2013, **7**, 8666–8672.

33 S. A. Thompson, I. A. Martínez, P. Haro-González, A. P. Adam, D. Jaque, J. B. Nieder and R. de la Rica, *ACS Photonics*, 2018, **5**, 2676–2681.

34 D. Täuber, A. Dobrovolsky, R. Camacho and I. G. Scheblykin, *Nano Lett.*, 2016, **16**, 5087–5094.

35 R. S. Gurjar, V. Backman, L. T. Perelman, I. Georgakoudi, K. Badizadegan, I. Itzkan, R. R. Dasari and M. S. Feld, *Nat. Med.*, 2001, **7**, 1245–1248.

36 L. Zhang, H. Li, Y. Yang, D. Yang, Y. Cui and G. Qian, *J. Mater. Chem. C*, 2022, **10**, 14915–14920.

37 H. He, E. Ma, Y. Cui, J. Yu, Y. Yang, T. Song, C.-D. Wu, X. Chen, B. Chen and G. Qian, *Nat. Commun.*, 2016, **7**, 11087.

38 H. Li, L. Zhang, Y. Yang, E. Hu, B. Li, Y. Cui, D. Yang and G. Qian, *Adv. Sci.*, 2022, **9**, 2200953.

39 Q. Wen, N. Malik, Y. Addadi, M. Weißenfels, V. Singh, L. J. W. Shimon, M. Lahav and M. E. van der Boom, *Angew. Chem., Int. Ed.*, 2023, **62**, e202214041.

40 H. Wang, S. I. Vagin, S. Lane, W. Lin, V. Shyta, W. R. Heinz, C. Van Dyck, A. J. Bergren, K. Gardner, B. Rieger and A. Meldrum, *Chem. Mater.*, 2019, **31**, 5816–5823.

41 Z. Zhou, C. Qiao, J. Yao, Y. Yan and Y. S. Zhao, *J. Mater. Chem. C*, 2022, **10**, 2551–2555.

42 K. Pei, J. Wu, M. Zhao, X. Feng, Y. Li, Y. Ma, H. Li and T. Zhai, *Adv. Opt. Mater.*, 2022, **10**, 2102143.

43 Q. Wen, S. Tenenholtz, L. J. W. Shimon, O. Bar-Elli, L. M. Beck, L. Houben, S. R. Cohen, Y. Feldman, D. Oron, M. Lahav and M. E. van der Boom, *J. Am. Chem. Soc.*, 2020, **142**, 14210–14221.

44 J. Yu, Y. Cui, C. Wu, Y. Yang, Z. Wang, M. O'Keeffe, B. Chen and G. Qian, *Angew. Chem., Int. Ed.*, 2012, **51**, 10542–10545.

45 A. P. Foster, J. P. Bradley, K. Gardner, A. B. Krysa, B. Royall, M. S. Skolnick and L. R. Wilson, *Nano Lett.*, 2015, **15**, 1559–1563.

46 D. M. Jameson and J. A. Ross, *Chem. Rev.*, 2010, **110**, 2685–2708.

This journal is © The Royal Society of Chemistry 2024

J. Mater. Chem. C, 2024, **12**, 2391–2397 | **2397**